

# Quantum Chemical Insight into 1,2-Shift Rearrangement in Bromination of Allylaryls

David Hardy, Stephen R. Isbel, Alejandro Bugarin,\* and Durgesh V. Wagle\*

Cite This: *ACS Omega* 2023, 8, 42311–42318

Read Online

ACCESS |



Metrics &amp; More

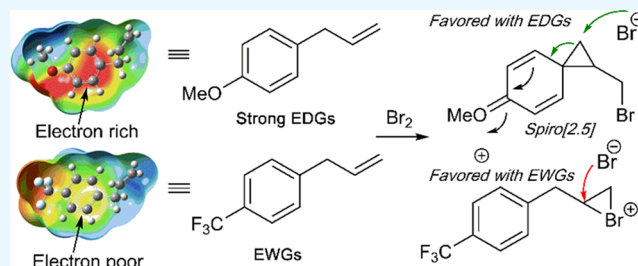


Article Recommendations



Supporting Information

**ABSTRACT:** In this work, we have provided mechanistic insight into the addition of bromine to an allylic double bond of allylaryl derivatives using experimental and DFT-based electronic structure methods. The experimental yields indicate the influence of the functional group on the aryl ring on the ratio of 1,2-dibromo and 1,3-dibromo adducts formed in the reaction. The optimized geometry and the electron density maps of the allylaryls and their cationic intermediates from DFT simulations revealed that electron-rich aryl rings promoted formation of cationic spiro[2.5] intermediate **II**, whereas electron-poor aryl rings resulted in formation of bromonium intermediate **I**. It was observed that electron-rich allylaryls promoted the 1,2-shift of the aryl ring that resulted in bond formation between the carbon atom (C1) on the aryl ring and the central carbon atom (C3) in the allylic double bond and formed spiro[2.5] intermediate **II**, a trend which was confirmed by harmonic oscillator model of aromaticity index. Also, Wiberg bond order analysis is in good agreement with the experimental work. Thermochemical analysis indicates that smaller C1...C3 distance resulted in favorable values for the difference in free energy change ( $\Delta\Delta G$ ). The favorable  $\Delta\Delta G$  values are a result of higher electron density on the aryl ring, making it more nucleophilic toward C3 carbon and promoting 1,2-shift that led to formation of the spiro[2.5] intermediate. Thus, the underlying mechanism indicates that the electron-rich allylaryls promote the formation of 1,3-dibromo compounds through formation and stabilization of the spiro[2.5] intermediate **II**.



## INTRODUCTION

Polymers and plastic have become an inseparable aspect of our everyday life, and polystyrene plays a central role in modernization of our society. Ever since its discovery in 1839, styrene in the form of polystyrene has found its way into everyday products as a versatile and inexpensive plastic material.<sup>1</sup> Styrene being a highly tailorable monomer can be transformed into polystyrene with unique properties such as being able to extrude in a glassy solid or in the form of lightweight foam.<sup>2</sup> Owing to the flexibility in the functional group chemistry on styrene monomers, and method involving copolymers, polystyrene with exceptional chemical and physical properties can be designed for specific applications, for instance, disposable packing in consumer products or heat-resistant polymer for industrial applications.<sup>3,4</sup> One such example of heat-resistant styrene is the  $\alpha$ -alkyl styrene which can also be functionalized and modified for further derivatization.<sup>5–7</sup> Unfortunately,  $\alpha$ -alkyl styrenes are difficult to produce due to a relative shortage of efficient synthetic methodologies. In most cases, aryl ketones are converted to terminal alkenes using Wittig reagents,<sup>8,9</sup> but this method is limited only to synthesis of  $\alpha$ -alkyl styrenes with simple alkyl groups.<sup>10–12</sup> Some methods of  $\alpha$ -alkyl styrene synthesis involving carbon-supported rhodium nanoparticle-assisted catalysis provide avenues for regioselective addition of branched or linear aldehydes.<sup>13</sup> However, other existing

methods require pre-existing  $\alpha$ -methyl or other reactive groups in place at the  $\alpha$  position. For example, new  $\alpha$ -alkyl styrenes are synthesized from  $\alpha$ -methylstyrenes by a regioselective elimination reaction via formation of tertiary alkyl radicals in a copper-mediated oxidation reaction.<sup>14</sup> Duan et al. synthesized  $\alpha$ -alkyl styrenes via enantioselective hydrogenation of  $\beta,\gamma$ -unsaturated phosphonates using Rh catalysts and chiral ferrocene-based monophosphoramidite ligands.<sup>15</sup> Bunrit et al. demonstrate that  $\alpha$ -alkyl styrenes can be synthesized in route to the synthesis of compounds having pyrrole substitution at  $\beta$ -position in benzyl or aryl groups.<sup>16</sup> Gupton and co-workers synthesized  $\alpha$ -alkyl styrenes by reaction of enolates with 2-aryl-3-(*N,N*-dimethylamino)-propene.<sup>17</sup> Highly regio- and stereo-selective methods to synthesize styrene derivatives have been illustrated in detail in our recently reported work on addition reactions to terminal alkenes.<sup>18,19</sup>

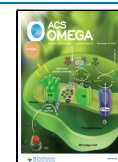
Recently, we reported the synthesis of  $\alpha$ -alkyl styrene using transition metal-free one-pot reaction conducted under mild

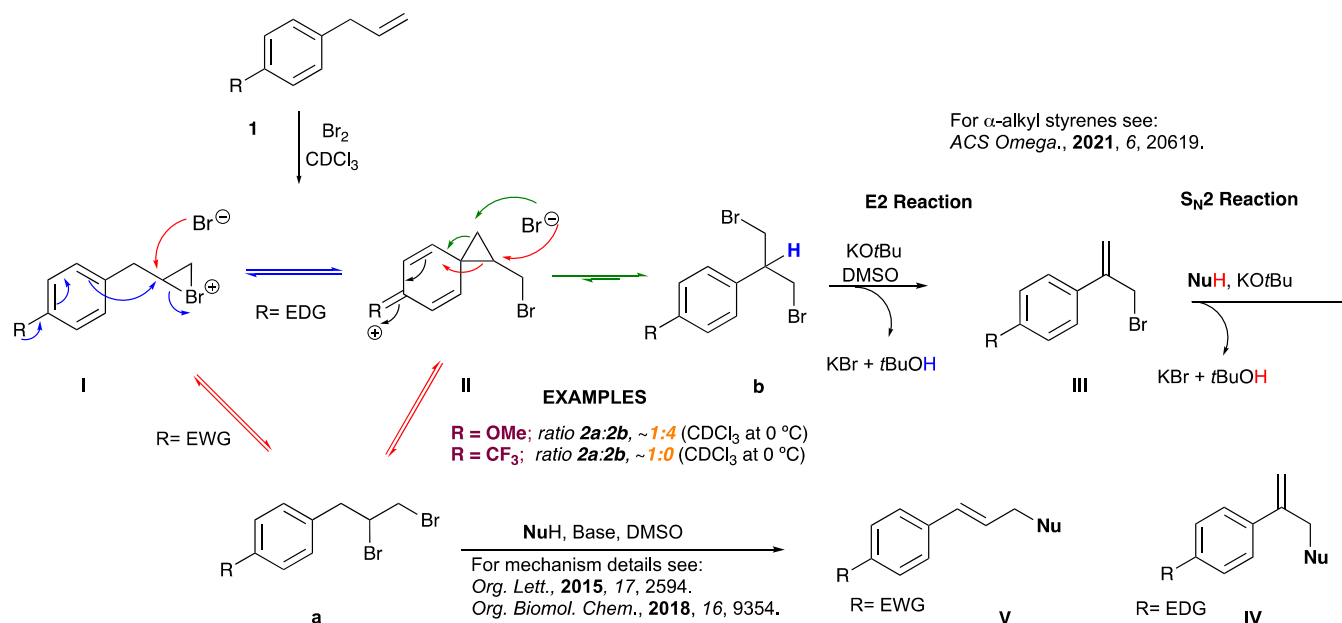
Received: June 24, 2023

Revised: October 9, 2023

Accepted: October 11, 2023

Published: November 1, 2023



Scheme 1. Proposed Mechanism for Formation of  $\alpha$ -Alkyl Styrene from Allylaryl

conditions.<sup>20–22</sup> Interestingly, this reaction resulted in a mixture of two distinct styrene derivatives, **a** and **b** (Scheme 1). Based on the experimental observations in our previously reported work and the bromine-mediated rearrangement reaction studies done by Dubois and Costa, it was proposed that allylaryl undergoes an alkene bromination to form bromonium intermediate **I**, which later on undergoes an intramolecular rearrangement, a 1,2-shift by the electron-rich aryl moiety to form the spiro[2.5] intermediate **II**.<sup>23,24</sup> The spiro[2.5] intermediate **II** can be ring-opened by a Br<sup>−</sup> anion on the three-membered ring to produce either a 2,3-dibromo derivative (**a**) or a 1,3-dibromo derivative (**b**). Furthermore, the 2,3-dibromo derivative (**a**) can also be formed by nucleophilic attack by a Br<sup>−</sup> anion on intermediate **I**. In this work, we have provided a detailed mechanistic insight into bromination of an allylic double bond in allylaryl derivatives using quantum chemical simulations based on density functional theory (DFT).

## EXPERIMENTAL METHODS

**General Information.** All reactions were carried out under air in oven-dried glassware with magnetic stirring at room temperature. All commercially obtained reagents were used as received. Solvents were dried and degassed from a JC Meyer company solvent purification system. Purification of reaction products was carried out by flash column chromatography using silica gel 60 (230–400 mesh). TLC visualization was accompanied with UV light. Concentration in vacuo refers to the removal of volatile solvent using a rotary evaporator attached to a dry diaphragm pump (10–15 mmHg) followed by pumping to a constant weight with an oil pump (<300 mTorr). <sup>1</sup>H NMR spectra were recorded at 400 MHz, and they are reported relative to CDCl<sub>3</sub> ( $\delta$  = 7.26). <sup>1</sup>H NMR coupling constants (*J*) are reported in hertz (Hz), and multiplicities are indicated as follows: s (singlet), d (doublet), t (triplet), and m (multiplet). Proton-decoupled <sup>13</sup>C NMR spectra were recorded at 100 MHz and reported relative to those of CDCl<sub>3</sub> ( $\delta$  = 77). IR experiments were recorded with neat samples on a Jasco FT/IR-4700 fitted with a diamond

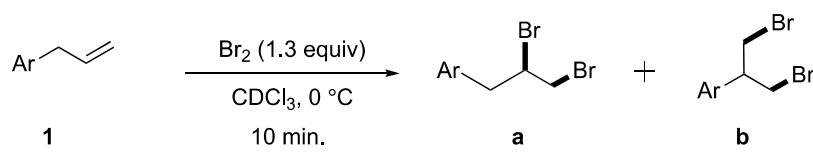
ATR sample plate. GCMS data were recorded on a Shimadzu GC-2010 plus System (GCMS-QP2010 SE).

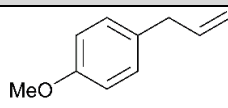
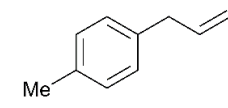
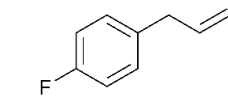
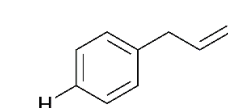
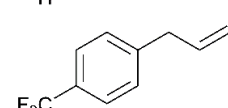
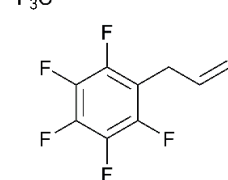
**Reagents and Materials.** The following starting materials were used as received from MilliporeSigma (St. Louis, MO): estragole (98%, cat. no. A29208), 4-allyltoluene (97%, cat. no. 706728), 1-allyl-4-fluorobenzene (97%, cat. no. 706787), allylbenzene (98%, cat. no. A29402), 1-allyl-4-(trifluoromethyl)benzene (95%, cat. no. 706779), and allylpentafluorobenzene (97%, cat. no. A34759). Hexanes (>98.5%, cat. no. H29220) and ethyl acetate (>99.5%, cat. no. E14520) were used as received from Fisher Scientific (Hanover Park, IL). Chloroform-d (99.8%, cat. no. DLM-7) was used as received from Cambridge Isotope Laboratory (Tewksbury, MA).

**General Method for the Preparation of Dibromo Compounds (2–7).** Allylbenzene (0.25 mmol, 1.0 equiv) and CDCl<sub>3</sub> (1.0 mL) were added to a 10 mL round-bottomed flask, equipped with a stir bar, at room temperature under air. The mixture was cooled down to 0 °C (ice bath), followed by dropwise addition of Br<sub>2</sub> (0.33 mmol, 17  $\mu$ L, 1.3 equiv). The reaction was stirred at 0 °C for 10 min. Then, the mixture was concentrated in vacuo. Purification by flash chromatography (SiO<sub>2</sub>, EtOAc/hexanes mixtures) provided pure dibromo products.

**Computational Methods.** The simulations were performed using Gaussian 16 software package, and molecular visualization was done using GaussView.<sup>25</sup> In this work, we used DFT-based M06-2X/6-31++G(d,p) theory and a basis set for prediction of geometry, electron density, and thermochemistry. This combination of theory and basis set has been effectively used in our earlier work to predict molecular geometry and thermochemical properties for ionic and molecular species.<sup>26–28</sup> Furthermore, M06 suite of density functionals has been successfully applied to the main group thermochemistry, noncovalent interactions, and excited states.<sup>29</sup> A scaling factor of 0.986 was used for the correction of vibrational frequencies calculated using the M06-2X/6-31++G(d,p) level of theory.<sup>29</sup> All simulations were carried out with no symmetry restrictions in the singlet ground state. The

**Table 1.** Comparative Study Depicting Reaction Yields and Ratio of 2,3-Dibromo (a) and 1,3-Dibromo (b) Formed after the Addition of Bromine to Allylaryls (EDG vs EWG)



entry	allylaryl	conv. <sup>b</sup> (%) <sup>c</sup>	a, <sup>1</sup> H NMR ratio <sup>d</sup>	b, <sup>1</sup> H NMR ratio <sup>d</sup>
1		>99 (94)	1	4
2		>99 (96)	2	1
3		>99 (90)	8.5	1
4		>99 (94)	11.5	1
5		>99 (98)	1	0
6		>99 (99)	1	0

<sup>a</sup>Reaction conditions: allylaryl **1a–f** (0.25 mmol, 1 equiv), bromine (0.33 mmol, 53 mg, 17  $\mu$ L, 1.3 equiv), in 1.0 mL of  $\text{CDCl}_3$  at 0  $^\circ\text{C}$  for 10 min. <sup>b</sup>Crude  $^1\text{H}$  NMR yield of reaction using mesitylene as the internal standard. <sup>c</sup>Isolated yield using silica gel flash chromatography. <sup>d</sup>Ratio determined by  $^1\text{H}$  NMR spectroscopy.

absence of imaginary frequency in the optimized structures indicates that they were a minima. The charge density was determined using charges from electrostatic potential maps using a grid-based method (CHELPG).<sup>30</sup> Dispersion corrections were accounted using the method developed by Grimme.<sup>31</sup> The harmonic oscillator model of aromaticity (HOMA) index and Wiberg bond order analysis were carried out using Multiwfn—a multifunctional wave function analyzer software package.<sup>32–34</sup> Change in the free energy ( $G$ ) of formation of intermediates of bromination was determined using the following equation:

$$\Delta G_{\text{intermediate}} = G_{\text{intermediate}} - G_{\text{allylaryl}} - G_{\text{Br}^+} \quad (1)$$

The difference in the change of free energy ( $\Delta\Delta G$ ) of formation of intermediate **I** and spiro[2.5] intermediate **II** for various allylaryl derivatives was obtained using eq 2 in which the allylaryl derivative with  $\text{R} = \text{H}$  was assigned a value of zero and  $\Delta\Delta G$  for other derivatives was calculated relative to the allylaryl derivative  $\text{R} = \text{H}$ . The allylaryl derivative  $\text{R} = -\text{H}$  was used as a baseline as it is the allylaryl derivative with an aryl ring having no substitutions other than the allylic group.

$$\Delta\Delta G_Y = \Delta G_{(\text{R}=\text{H})} - \Delta G_{(\text{R}=\text{Y})} \quad (2)$$

where  $\text{Y} = -\text{OMe}$ ,  $-\text{Me}$ ,  $-\text{F}$ ,  $-\text{CF}_3$ , and pentafluoro derivative of allylaryl.

## RESULTS AND DISCUSSION

The experimental evidence strongly pointed toward the influence of the functional group on the aryl ring in allylaryl derivatives on the outcome of the bromination reaction, as indicated by the ratio of 2,3-dibromo (**a**) and 1,3-dibromo (**b**) formed in the reaction, see Table 1. It was observed that the presence of the strong electron-withdrawing group (EWG) such as  $-\text{CF}_3$  on the aryl ring or the lack of electron density of the aryl ring (pentafluoro derivative) exclusively results in formation of **a** in the reaction. On the other hand, because of the presence of a strong electron-donating group (EDG) on the aromatic ring such as  $-\text{OMe}$ , **a** is formed as a minor product and **b** is the major product. This ratio of **a** and **b** gradually favored formation of **a** over **b** as the functional group gradually switched from a strong EDG to a moderate EDG/EWG to a strong EWG, see Table 1.

According to the proposed mechanism in Scheme 1, the 1,3-dibromo adduct is produced when the spiro[2.5] intermediate **II** is formed during the reaction. The experimental ratios of **a** and **b** are a function of the amount of spiro[2.5] intermediate

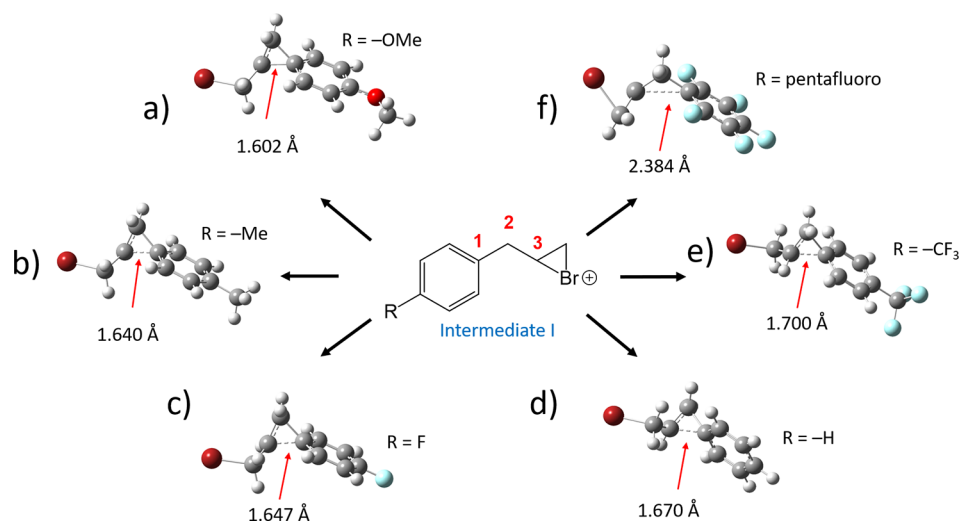


**Figure 1.** Extent of formation of intermediate II from geometrical optimization of bromonium cation intermediate I for various allylaryl derivatives: (a)  $-OMe$ , (b)  $-Me$ , (c)  $-F$ , (d)  $-H$ , (e)  $-CF_3$ , and (f) pentafluoro. The simulations were performed with the M06-2X/6-31++G(d,p) theory and basis set.

II formed during the reaction. Therefore, in order to understand the underlying factors that influence the formation of intermediate I and spiro[2.5] intermediate II, we investigated the influence of the functional group on the electronic environment of the aryl ring in allylaryl derivatives using the DFT-based method M06-2X/6-31++G(d, p) theory and basis set. The geometrical optimization of bromonium intermediate I (Figure 1, center) of allylaryl derivatives was used as a starting point for this investigation as it is the first intermediate formed during addition of bromine to alkenes. It was observed that the optimized geometry of the starting structure of intermediate I either had rearranged to resemble more like spiro [2.5] intermediate II or resemble more like intermediate I. The optimized structures showed that the extent of rearrangement was dependent on the functional group present on the aryl ring. This extent was measured in terms of the distance between carbon atoms C1 and C3 (C1...C3) as shown in Figure 1. The C1...C3 is crucial for the formation of the three-membered ring in the spiro[2.5] intermediate II. The influence of the nature of the R-group on the distance between C1 and C3 can be clearly observed in Figure 1. For instance, in the presence of strong EDG like  $-OMe$ , there is a bond formation between C1 and C3 atoms with a bond length of 1.602 Å (Figure 1a), leading to formation of the spiro [2.5] intermediate II. However, this bond distance gradually increases (weakens) as the nature of the functional group gradually shifts from EDG to EWG with longest C1...C3 distance of 2.384 Å in the case of pentafluoro derivative. The interatomic distance between C1...C3 in allylaryl derivatives increases in the following order:  $-OMe < -Me < -F < -H < -CF_3 < \text{pentafluoro}$ , see Figure 1 and Table 2. Alternatively, the C3...Br distance had an inverse relationship to C1...C3, with shortest C3...Br distance of 2.066 Å in the pentafluoro derivative, which indicates the preference to form bromonium intermediate I, whereas derivatives that form spiro[2.5] intermediate II had a significantly longer C3...Br distance, see Table 2. Thus, the optimized structures clearly indicate the formation of the spiro[2.5] intermediate II in allylaryl derivatives  $R = -OMe, -Me, -F, \text{ and } -H$ , which results in the formation of the 1,3-dibromo compound b, whereas the  $-CF_3$  and pentafluoro derivatives resembled

**Table 2. Values of the Harmonic Oscillator Model of Aromaticity (HOMA) Index for the Allylaryls, Carbocation Intermediates, and the Difference in HOMA Index between Allylaryls and Cationic Intermediates**

derivatives	harmonic oscillator model of aromaticity (HOMA)		
	allylaryls (A)	cationic intermediates (C)	difference (A-C)
pentafluoro	0.9989	0.9949	0.0040
$-CF_3$	0.9865	0.9023	0.0842
$-F$	0.9881	0.8217	0.1664
$-H$	0.9857	0.8743	0.1114
$-Me_3$	0.9816	0.7995	0.1821
$-OMe$	0.9819	0.6136	0.3683

bromonium intermediate I that leads to the formation of the 2,3-dibromo compound a in the reaction. These observations from the optimized structures of intermediates I and II are in good agreement with experimentally observed trends indicating gradual change in the ratio of formation of a:b such as (1:4), (2:1), (8.5:1), (11.5:1), (1:0), and (1:0) for allylaryl derivatives with  $R = -OMe, -Me, -F, -H, -CF_3,$  and pentafluoro derivatives, respectively (Table 1).

Figures 1 and 2 indicates that this order of electron density is inversely correlated with the distance between C1 and C3 carbon atoms. The higher is the electron density on the aryl ring, the smaller the distance between C1 and C3, which is key to the formation of the spiro[2.5] intermediate II. For instance, the C1...C3 distance in allylaryl derivatives ( $-OMe$ ) with highest electron density in the aryl ring is 1.602 Å, while the C1...C3 distance in the pentafluoro derivative with lowest electron density in the phenyl ring

In order to understand the underlying factors responsible for the formation of the spiro [2.5] intermediate II, we investigated the electronic environment of starting allylaryl derivatives (I) in Scheme 1. The analysis of the electronic environment was performed by estimation of atomic charges using CHarges from Electrostatic Potentials using a Grid-based (CHELPG) method developed by Breneman and Wiberg.<sup>30</sup> In Figure 2, the electron density maps indicate a gradual decrease in the electron density on the phenyl ring of the allylaryl

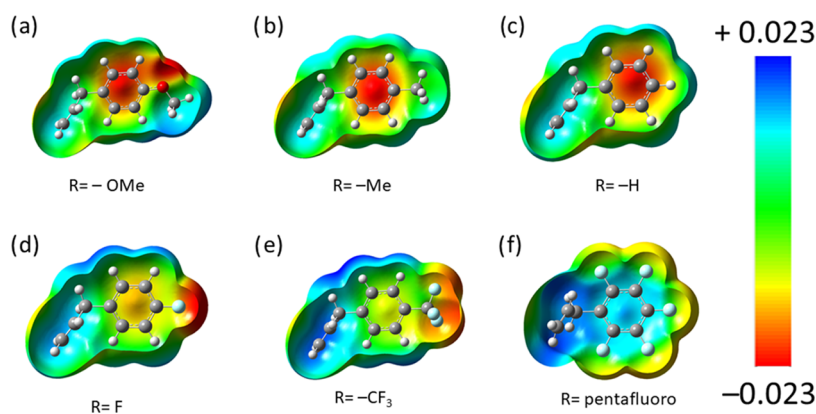


**Figure 2.** Electron density map of allylaryl derivatives obtained from electrostatic potential using the CHELPG method at the M06-2X/6-31++G(d,p) theory and basis set. The allylaryl derivatives are as follows: (a)  $-OMe$ , (b)  $-Me$ , (c)  $-H$ , (d)  $-F$ , (e)  $-CF_3$ , and (f) pentafluoro.

derivatives in the following order:  $-OMe > -Me > -H > -F > -CF_3 > \text{pentafluoro}$ . A comparison between is 2.384 Å.

In order to further investigate the influence of functional groups on the 1,2-shift rearrangement reaction, we estimated the HOMA index for allylaryls and cationic intermediates. The HOMA index is a widely used molecular descriptor that is based on the geometrical aromaticity of the compounds. This index assigns a value to the molecules indicating their aromatic character, with benzene as a standard with a HOMA value of 1 indicating that it is perfectly aromatic, whereas a compound with a HOMA value of 0 indicates that it is not aromatic.<sup>35</sup> The HOMA values of allylaryls ranged between 0.9816 for  $-Me$  and 0.9989 for pentafluoro derivative, indicating that all allylaryl derivatives are significantly aromatic (Table 2). Interestingly, cationic intermediates exhibited significant loss of aromatic character in derivatives containing EDG as indicated by lower values for HOMA index. The loss of aromatic character was the most dramatic in the case of cation intermediates with strong EDG such as  $R = -OMe$ , indicating significant involvement of the aromatic ring and resulting in formation of the spiro[2.5] intermediate II. On the contrary, the cationic intermediate with an electron-deficient aryl ring such as the pentafluoro derivative exhibited little to no loss of aromatic character compared to its starting allylaryl, indicating no involvement of the aryl ring and promotion of formation of cationic intermediate I.

Additionally, we performed Wiberg bond order (BO) analysis to investigate the strength of the  $C1 \cdots C3$  interaction in the cationic intermediates. Table 3 depicts the  $C1 \cdots C3$  interaction bond distance and the corresponding bond order. It can be clearly observed that the shorter the distance between the  $C1$  and  $C3$  carbon atoms, the higher is the bond order. The cationic derivative with the  $-OMe$  group exhibited a BO

of 0.8, giving the  $C1 \cdots C3$  interaction a single bond-like character, whereas the pentafluoro derivative exhibited a BO of 0.12, an indication of a very weak  $C1 \cdots C3$  interaction. In other words, EDGs on the aryl ring enhanced the electron density and resulted in shorter distance between the  $C1 \cdots C3$  carbon atoms, thus promoting 1,2-shift and the formation of the spiro[2.5] intermediate II; whereas, the derivatives containing EWGs lack electron density and thus favor conservation of bromonium intermediate I. This highlights the influence of EDGs and EWGs on the extent of formation of intermediates I and II.

Although it is clear that the electron density on the phenyl ring of the allylaryl derivative plays a significant role in the outcome of the bromination reaction, there are exceptions. For instance, in monofluoro derivative of allylaryl, despite a lower electron density in the phenyl ring compared to the unsubstituted derivative (Figure 2c,d), the former has a slightly shorter  $C1 \cdots C3$  distance of 1.647 Å compared to the latter with a  $C1 \cdots C3$  distance of 1.670 Å (Figure 1c,d). This indicates that there is a greater chance of formation of spiro [2.5] intermediate II in monofluorinated derivative compared to unsubstituted derivative. This was confirmed from the experimental data in Table 1, which indicate the formation of higher amounts of **b** in the monofluorinated derivative compared to the unsubstituted derivative. Upon further investigation, the electrostatic potential (ESP) charge analysis indicated a charge of  $-0.255$  on the fluorine atom in the monofluorinated derivative of allylaryl, suggesting that fluorine is pulling the electron density due to the inductive effect. On the other hand, the Wiberg BO value of 1.21 for the  $C-F$  bond in the monofluorinated derivative indicated a partial double bond character; this BO increases to 1.32 in the spiro[2.5] intermediate II, which is suggestive of the resonance effect in action. Interestingly, the ESP charge on the F atom in the spiro[2.5] intermediate II is reduced to  $-0.18$ , which is an indication that fluorine loses the overall electron density during the rearrangement reaction. Furthermore, there is a bigger difference in the HOMA index value of the allylaryl and the spiro[2.5] intermediate in the case of the monofluorinated derivative compared to the unsubstituted derivative; see Table 2. This is indicative of higher involvement of the benzene ring in the 1,2-shift rearrangement in the monofluorinated derivative compared to the unsubstituted allylaryl derivative. Overall, the analysis indicates that the resonance effect dominates over the inductive effect in the monofluorinated

**Table 3.** Table Comparing the  $C1 \cdots C3$  Interaction Distance and the Wiberg Bond Order Values

derivatives	$C1 \cdots C3$ distance (Å)	$C3 \cdots Br$ distance (Å)	Wiberg bond order
pentafluoro	2.384	2.066	0.12
$-CF_3$	1.700	2.739	0.65
$-F$	1.647	2.765	0.73
$-H$	1.670	2.754	0.69
$-Me$	1.640	2.772	0.74
$-OMe$	1.602	2.791	0.80

derivative, thus leading to the formation of a tighter spiro[2.5] intermediate **II** compared to the unsubstituted derivative.

The thermochemical analysis of a system provides critical insight into the feasibility of a process by gauging the stability of the intermediates and the products with respect to starting materials involved in the chemical process. It also helps us in understanding the relative stability of various reaction intermediates that are involved in the systems under consideration and provides mechanistic insight. The free energy of formation of reaction intermediates **I** and **II** from **1** was calculated using eq 1, which revealed that it is a thermodynamically favorable process (Table 4). Further, we

**Table 4.** Calculated Change in Free Energy ( $\Delta G$ ) of Formation of Carbocation Intermediate for Various Allylaryl Derivatives and the Relative Difference in the Free Energy Change ( $\Delta\Delta G$ ) of Formation of Carbocation Intermediate among Allylaryl Derivatives

allylaryl derivative	$\Delta G$ (kcal/mol) carbocation intermediate	$\Delta\Delta G$ (kcal/mol) between carbocation intermediate
pentafluoro	-105.27	14.47
-CF <sub>3</sub>	-109.82	9.92
-F	-118.48	1.26
-H	-119.74	0
-Me	-125.19	-5.45
-OMe	-132.22	-12.48

calculated the difference in the free energy change ( $\Delta\Delta G$ ) of intermediates of various allylaryl derivatives using eq 2. During this calculation, we used the allylaryl derivative R = H as a baseline ( $\Delta\Delta G = 0$ ) with respect to which  $\Delta\Delta G$  for other allylaryl derivatives containing EDGs and EWGs was calculated. It was noted that the  $\Delta\Delta G$  values for allylaryl derivatives with EDGs such as R = -OMe and -Me were lower than that of the allylaryl derivative R = -H by 12.48 and 5.45 kcal/mol, respectively. However, in the case of allylaryl derivatives with EWGs such as R = -F, -CF<sub>3</sub>, and pentafluoro, the  $\Delta\Delta G$  values were higher than that of R = -H by 1.26, 9.92, and 14.47 kcal/mol, respectively (Table 4). This trend of  $\Delta\Delta G$  of allylaryl derivatives is inversely related to the C1...C3 distance in the optimized structures of the cationic intermediates. In Figure 3, it can be clearly observed that the allylaryl cationic intermediates with shorter C1...C3 distance have low  $\Delta\Delta G$  values, whereas the longer distance between C1...C3 leads to higher values in  $\Delta\Delta G$ . From this correlation, the shorter C1...C3 distance results in a better interaction of the C3 atom with the aryl ring and enhanced charge distribution that leads to stabilization of the spiro[2.5]

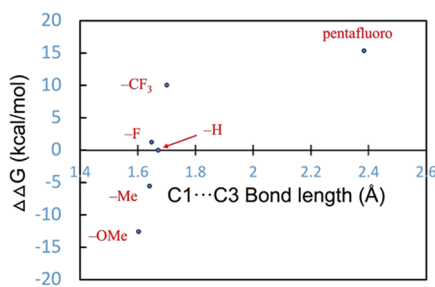


**Figure 3.** Plot depicting the correlation between the interatomic distance between carbon atoms C1 and C3 and  $\Delta\Delta G$  of various allylaryl derivatives.

intermediate **II** and lower  $\Delta\Delta G$  values, whereas the longer C1...C3 distance reduced the interaction of C3 carbon atom with the aryl ring and leads to formation of a structure that resembles intermediate **I**, which has higher  $\Delta\Delta G$  values. Interestingly, from the plot, it can also be observed that for the pentafluoro derivative, the  $\Delta\Delta G$  value does not rise proportionally with the increase in the C1...C3 distance of 2.384 Å. This is an indication that for the reaction intermediates of bromination of allylaryl derivatives containing EWGs that are stronger than -CF<sub>3</sub>, the  $\Delta\Delta G$  value attains a plateau. This is because the C1...C3 distance reached the limit of maximum distance between carbon atoms in a three-atom system with bond angles between C1-C2-C3 getting close to a tetrahedral angle of 104.74 degrees.

In summary, the optimized geometries of the cationic intermediates indicate that the allylaryl derivatives containing EDGs formed a spiro[2.5] intermediate **II** as indicated by the bond formation between the carbon atom C1 on the aryl ring and the carbon atom C3 of the allylic double bond. The C1...C3 interaction distance was shortest in allylaryl compounds with strong EDG such as -OMe. A gradual shift in the nature of the functional group from EDG to EWG resulted in elongation/weakening of C1...C3 interaction with no interaction in the case of the aryl ring with strong EWG. This trend was in agreement with experimentally observed results indicating the formation of the 1,3-dibromo product in reaction with allylaryl derivatives containing EDG and their gradual decrease in the case of allylaryls containing EWG. The electron density mapping of the allylaryls indicates inverse relationship between the electron density on the aryl ring and the interaction distance between the C1 and C3 carbon atoms, clearly indicating that electron-rich aryl ring promotes formation of spiro[2.5] intermediate **II**. The HOMA index indicated that the phenyl rings with EDG participated in the 1,2-shift and promoted the formation of spiro[2.5] intermediate **II**. The Wiberg BO analysis agreed with the trend for C1 and C3 interaction distance with higher BO values for shorter C1...C3 distance. The thermochemical analysis of the cationic intermediates indicated that the allylaryl derivatives with EDG exhibited lower  $\Delta\Delta G$  values compared to the derivatives with EWG. The lower  $\Delta\Delta G$  values in the allylaryl derivative containing EDG arise from the involvement of the aryl moiety in stabilization of the cationic intermediate and formation of spiro[2.5] intermediate **II**, which is absent in the case of derivatives containing EWG. Therefore, experimental observations coupled with computational insight on geometry analysis, electron density mapping, and thermochemical analysis indicate that the aryl ring in the electron-rich allylaryl systems undergoes a 1,2-shift to produce spiro[2.5] intermediates, which then form 1,3-dibromo compounds.

## ■ ASSOCIATED CONTENT

### Supporting Information

The Supporting Information is available free of charge at <https://pubs.acs.org/doi/10.1021/acsomega.3c04513>.

Dibromide Compounds, Experimental Data, Cartesian coordinates (PDF)

## AUTHOR INFORMATION

### Corresponding Authors

Alejandro Bugarin – Florida Gulf Coast University, Fort Myers, Florida 33965, United States; [orcid.org/0000-0001-8504-355X](https://orcid.org/0000-0001-8504-355X); Email: [abugarin@fgcu.edu](mailto:abugarin@fgcu.edu)

Durgesh V. Wagle – Florida Gulf Coast University, Fort Myers, Florida 33965, United States; [orcid.org/0000-0002-2522-0670](https://orcid.org/0000-0002-2522-0670); Email: [dwagle@fgcu.edu](mailto:dwagle@fgcu.edu)

### Authors

David Hardy – Florida Gulf Coast University, Fort Myers, Florida 33965, United States; [orcid.org/0000-0003-4029-4595](https://orcid.org/0000-0003-4029-4595)

Stephen R. Isbel – Florida Gulf Coast University, Fort Myers, Florida 33965, United States; [orcid.org/0009-0002-8171-9393](https://orcid.org/0009-0002-8171-9393)

Complete contact information is available at:

<https://pubs.acs.org/10.1021/acsomega.3c04513>

### Author Contributions

A.B. and D.V.W. conceived, designed the work, and analyzed the data. D.H. performed the simulations, and S.R.I. conducted the experimental part. The manuscript was written by A.B. and D.V.W. All authors have given approval to the final version of the manuscript.

### Funding

This original research article was supported by the National Institute of General Medical Sciences (NIGMS) of the National Institutes of Health (NIH) under award number 1R15GM141726-01.

### Notes

The authors declare no competing financial interest.

## ACKNOWLEDGMENTS

The authors would like to acknowledge the College of Arts and Science and the high-performance computing facility at Florida Gulf Coast University and Seidler Fellowship for partially supporting this work.

## REFERENCES

- (1) Simon, E. Ueber den flüssigen Storax (*Styrax liquidus*). *Ann. Pharm.* **1839**, *31* (3), 265–277.
- (2) Modern Styrenic Polymers: Polystyrenes and Styrenic Copolymers. In *Wiley Series in Polymer Science*; Scheirs, J.; Priddy, D. B., Eds.; John Wiley & Sons, Ltd: Chichester, UK, 2003; pp i–xxxiii.
- (3) Hersberger, A. B.; Reid, J. C.; Heiligmann, R. G. Polymerization of Alpha-Methylstyrene. *Ind. Eng. Chem.* **1945**, *37*, 1073–1078.
- (4) Perrier, S. 50th Anniversary Perspective: RAFT Polymerization—A User Guide. *Macromolecules* **2017**, *50* (19), 7433–7447.
- (5) Sakurada, Y. Polymerization of  $\alpha$ -Methylstyrene with Al(C<sub>2</sub>H<sub>5</sub>)<sub>3</sub>-TiCl<sub>4</sub> Catalyst. *J. Polym. Sci., Part A: Gen. Pap.* **1963**, *1* (7), 2407–2418.
- (6) Banerjee, S.; Paira, T. K.; Mandal, T. K. Control of Molecular Weight and Tacticity in Stereospecific Living Cationic Polymerization of  $\alpha$ -Methylstyrene at 0 °C Using FeCl<sub>3</sub>-Based Initiators: Effect of Tacticity on Thermal Properties. *Macromol. Chem. Phys.* **2013**, *214* (12), 1332–1344.
- (7) Ayat, M.; Bensaada, N.; Belbachir, M.; Harrane, A.; Meghabar, R. Synthesis and Characterization of Poly( $\alpha$ -Methylstyrene) by Cationic Polymerization Using a New Solid Ecological Catalyst. *Orient. J. Chem.* **2015**, *31* (4), 2115–2123.
- (8) Wittig, G.; Geissler, G. Zur Reaktionsweise Des Pentaphenyl-Phosphors Und Einiger Derivate. *Justus Liebig's Ann. Chem.* **1953**, *580* (1), 44–57.
- (9) Wittig, G.; Schöllkopf, U. Über Triphenyl-phosphin-methylene als olefinbildende Reagenzien (I. Mitteil. *Chem. Ber.* **1954**, *87* (9), 1318–1330.
- (10) Zhang, S.; Bedi, D.; Cheng, L.; Unruh, D. K.; Li, G.; Findlater, M. Cobalt(II)-Catalyzed Stereoselective Olefin Isomerization: Facile Access to Acyclic Trisubstituted Alkenes. *J. Am. Chem. Soc.* **2020**, *142* (19), 8910–8917.
- (11) Yang, S.; Zhu, S.-F.; Guo, N.; Song, S.; Zhou, Q.-L. Carboxy-Directed Asymmetric Hydrogenation of  $\alpha$ -Alkyl- $\alpha$ -Aryl Terminal Olefins: Highly Enantioselective and Chemoselective Access to a Chiral Benzylmethyl Center. *Org. Biomol. Chem.* **2014**, *12* (13), 2049–2052.
- (12) Pine, S. H.; Shen, G. S.; Hoang, H. Ketone Methylenation Using the Tebbe and Wittig Reagents - A Comparison. *Synthesis* **1991**, *1991* (02), 165–167.
- (13) Zhang, X.; Zhang, H.; Guo, G.; Sun, Q.; He, X.; Ji, H. Phosphorus-Doped Carbon-Supported Rh Nanoparticles for the Hydroformylation of Styrene with High Regioselectivity. *Ind. Eng. Chem. Res.* **2023**, *62*, 8174.
- (14) Wang, C.; Liu, R.-H.; Tian, M.-Q.; Hu, X.-H.; Loh, T.-P. Regioselective Copper-Catalyzed Oxidative Coupling of  $\alpha$ -Alkylated Styrenes with Tertiary Alkyl Radicals. *Org. Lett.* **2018**, *20* (13), 4032–4035.
- (15) Duan, Z.-C.; Hu, X.-P.; Zhang, C.; Wang, D.-Y.; Yu, S.-B.; Zheng, Z. Highly Enantioselective Rh-Catalyzed Hydrogenation of  $\beta,\gamma$ -Unsaturated Phosphonates with Chiral Ferrocene-Based Monophosphoramidite Ligands. *J. Org. Chem.* **2009**, *74* (23), 9191–9194.
- (16) Bunrit, A.; Sawadjoon, S.; Tšupova, S.; Sjöberg, P. J. R.; Samec, J. S. M. A General Route to  $\beta$ -Substituted Pyrroles by Transition-Metal Catalysis. *J. Org. Chem.* **2016**, *81* (4), 1450–1460.
- (17) Gupton, J. T.; Krolkowski, D.; Rusler, M. The Reaction of Quaternary Ammonium Salts Derived From 2 Aryl-3-(N,N-Dimethylamino)-1-Propenes with Some Enoate Anions. *Synth. Commun.* **1989**, *19* (13–14), 2415–2421.
- (18) Ojo, O. S.; Miranda, O.; Baumgardner, K. C.; Bugarin, A. Practical Regio- and Stereoselective Azidation and Amination of Terminal Alkenes. *Org. Biomol. Chem.* **2018**, *16* (48), 9354–9358.
- (19) Huang, X.; Fulton, B.; White, K.; Bugarin, A. Metal-Free, Regio- and Stereoselective Synthesis of Linear (E)-Allylic Compounds Using C, N, O, and S Nucleophiles. *Org. Lett.* **2015**, *17* (11), 2594–2597.
- (20) Ojo, O. S.; Bugarin, A. One-Pot Synthesis of  $\alpha$ -Alkyl Styrene Derivatives. *ACS Omega* **2021**, *6* (31), 20619–20628.
- (21) Blé-González, E. A.; Isbel, S. R.; Ojo, O. S.; Hillesheim, P. C.; Zeller, M.; Bugarin, A. Regiodivergent Sulfonylation of Terminal Olefins via Dearomative Rearrangement. *New J. Chem.* **2023**, *47*, 17020–17025.
- (22) Isbel, S. R.; Bugarin, A. Synthesis of a New  $\alpha$ -Azidomethyl Styrene from Saffrole via a Dearomative Rearrangement. *Molbank* **2023**, *2023* (3), M1713.
- (23) Dubois, J. E.; Toullec, J.; Fain, D. Addition Du Brome Sur l'allyl-4 Anisole via Un Intermediaire Phenonium. *Tetrahedron Lett.* **1973**, *14* (49), 4859–4860.
- (24) Costa, P. R. R. Saffrol e Eugenol: Estudo Da Reatividade Química e Uso Em Síntese de Produtos Naturais Biologicamente Ativos e Seus Derivados. *Quim. Nova* **2000**, *23* (3), 357–369.
- (25) Frisch, M. J.; Trucks, G. W.; Schlegel, H. B.; Scuseria, G. E.; Robb, M. A.; Cheeseman, J. R.; Scalmani, G.; Barone, V.; Petersson, G. A.; Nakatsuji, H.; Li, X.; Caricato, M.; Marenich, A. V.; Bloino, J.; Janesko, B. G.; Gomperts, R.; Mennucci, B.; Hratchian, H. P.; Ortiz, J. V.; Izmaylov, A. F.; Sonnenberg, J. L.; Williams-Young, D.; Ding, F.; Lipparini, F.; Egidi, F.; Goings, J.; Peng, B.; Petrone, A.; Henderson, T.; Ranasinghe, D.; Zakrzewski, V. G.; Gao, J.; Rega, N.; Zheng, G.; Liang, W.; Hada, M.; Ehara, M.; Toyota, K.; Fukuda, R.; Hasegawa, J.; Ishida, M.; Nakajima, T.; Honda, Y.; Kitao, O.; Nakai, H.; Vreven, T.; Throssell, K.; Montgomery, J. A., Jr.; Peralta, J. E.; Ogliaro, F.;

Bearpark, M. J.; Heyd, J. J.; Brothers, E. N.; Kudin, K. N.; Staroverov, V. N.; Keith, T. A.; Kobayashi, R.; Normand, J.; Raghavachari, K.; Rendell, A. P.; Burant, J. C.; Iyengar, S. S.; Tomasi, J.; Cossi, M.; Millam, J. M.; Klene, M.; Adamo, C.; Cammi, R.; Ochterski, J. W.; Martin, R. L.; Morokuma, K.; Farkas, O.; Foresman, J. B.; Fox, D. J. *Gaussian 16*, Revision A.03; Gaussian, Inc.: Wallingford CT, 2016.

(26) Wagle, D. V.; Deakne, C. A.; Baker, G. A. Quantum Chemical Insight into the Interactions and Thermodynamics Present in Choline Chloride Based Deep Eutectic Solvents. *J. Phys. Chem. B* **2016**, *120* (27), 6739–6746.

(27) Anderson, G. I.; Hardy, D.; Hillesheim, P. C.; Wagle, D. V.; Zeller, M.; Baker, G. A.; Mirjafari, A. Anticancer Agents as Design Archetypes: Insights into the Structure–Property Relationships of Ionic Liquids with a Triarylmethyl Moiety. *ACS Phys. Chem. Au* **2023**, *3* (1), 94–106.

(28) Recker, E. A.; Hardy, D.; Anderson, G. I.; Mirjafari, A.; Wagle, D. V. Covalently Linked Hydrogen Bond Donors: The Other Side of Molecular Frustration in Deep Eutectic Solvents. *J. Chem. Phys.* **2021**, *155* (8), No. 084502.

(29) Zhao, Y.; Truhlar, D. G. The M06 Suite of Density Functionals for Main Group Thermochemistry, Thermochemical Kinetics, Noncovalent Interactions, Excited States, and Transition Elements: Two New Functionals and Systematic Testing of Four M06-Class Functionals and 12 Other Functionals. *Theor. Chem. Acc.* **2008**, *120* (1), 215–241.

(30) Breneman, C. M.; Wiberg, K. B. Determining Atom-Centered Monopoles from Molecular Electrostatic Potentials. The Need for High Sampling Density in Formamide Conformational Analysis. *J. Comput. Chem.* **1990**, *11* (3), 361–373.

(31) Grimme, S. Semiempirical GGA-Type Density Functional Constructed with a Long-Range Dispersion Correction. *J. Comput. Chem.* **2006**, *27* (15), 1787–1799.

(32) Wiberg, K. B. Application of the Pople-Santry-Segal CNDO Method to the Cyclopropylcarbinyl and Cyclobutyl Cation and to Bicyclobutane. *Tetrahedron* **1968**, *24* (3), 1083–1096.

(33) Kruszewski, J.; Krygowski, T. M. Definition of Aromaticity Basing on the Harmonic Oscillator Model. *Tetrahedron Lett.* **1972**, *13* (36), 3839–3842.

(34) Lu, T.; Chen, F. Multiwfn: A Multifunctional Wavefunction Analyzer. *J. Comput. Chem.* **2012**, *33* (5), 580–592.

(35) Dobrowolski, J. Cz. Three Queries about the HOMA Index. *ACS Omega* **2019**, *4* (20), 18699–18710.